Complex Pattern Formation in Solutions of Protein and Mixed Salts Using Dehydrating Sessile Droplets

Complex pattern formation in solutions of protein and mixed salts using dehydrating sessile droplets

Binita Pathak[1], John Christy[2*], Khellil Sefiane[2,4] and Devrim Gozuacik[3]

[1]Department of Mechanical Engineering, Indian Institute of Technology, BHU, Varanasi-221005, India
[2]School of Engineering, The University of Edinburgh, Kings Buildings, Edinburgh EH9 3JL, United Kingdom
[3]Koç University, School of Medicine, KUTTAM Research Center for Translational Medicine, Topkapı-Zeytinburnu 34010 Istanbul, Turkey
[4]Tianjin Key Lab of Refrigeration Technology, Tianjin University of Commerce, Tianjin City 300134, PR China

ABSTRACT

A sessile droplet of complex fluid exhibits several stages of drying leading to the formation of a final pattern on the substrate. We report such pattern formation in dehydrating droplets of protein (BSA) and salts ($MgCl_2$ and KCl) at various concentrations of the two components (protein and salts) as part of a parametric study for the understanding of complex patterns of dehydrating biofluid droplets (blood and urine), which will eventually be used for diagnosis of bladder cancer. The exact analysis of the biofluid patterns will require a rigorous parametric study, however, the current work provides an initial understanding of the effect of the basic components present in a bio-fluid droplet. Arrangement of the protein and the salts, due to evaporation, leads to the formation of some very distinctive final structures at the end of the droplet lifetime. Furthermore, these structures can be manipulated by varying the initial ratio of the two components in the solution. $MgCl_2$ forms chains of crystals beyond a threshold initial concentration of protein (> 3% by wt.). However, the formation of such a crystal is also limited by the maximum concentration of the salt initially present in the droplet (≤ 1% by wt.). On the other hand, KCl forms dendritic and rectangular crystals in the presence of BSA. The formation of these crystals also depends upon the relative concentration of salt and protein in the droplet. We also investigated the dried-out patterns in dehydrating droplets of mixed salts ($MgCl_2$+KCl) and protein. The patterns can be tuned from continuous dendritic structure to snow-flake type structure just by altering the initial ratio of the two salts in the mixture, keeping all other parameters constant.

INTRODUCTION

Organization of bio-molecules is of significant importance in biological systems. For instance,

proteins consist of amino acid units which are organized to acquire minimum free energy configuration for normal functioning. However, the units can also organize abnormally to an unstable state leading to several complications in the body [1]. Several diseases like Huntington's, Alzheimer's, Parkinson's, etc. are associated with protein aggregation [2]. Therefore, it is crucial to understand and control the process of interaction and aggregation between protein molecules to prevent and cure various diseases [1]. However, it is difficult to attain precise control of self-assembly in such bio-molecules. Understanding of individual protein conformation and crystallization (on a molecular level) requires a rigorous and time-consuming process which includes isolation of protein molecules by purification and expression. An evaporating sessile droplet is an excellent platform to study such structural arrangement. Evaporation of droplets is a simple experimental approach which can be used for diagnosis of diseases.

A dehydrating droplet of a complex fluid placed on a substrate leads to the formation of complicated identifiable structures (patterns) on the substrate at the end of the drying process. These patterns can be utilized for diagnosis of various diseases [3-11]. For instance, Martusevich et. al observed some distinctive crystal characteristics which can be used to identify the presence of viral hepatitis in patient's blood serum [4]. Brutin et. al also identified some significant differences in the patterns of dehydrating blood droplets between those obtained from a healthy person and those from a person with disease such as anemia and hyperlipidemia [7]. The differences in the pattern formation were explained on the basis of the flow field developed inside the droplets. A more detailed analysis was later performed by Sobac and Brutin, delineating the different stages involved during drying of such blood droplets [12].

As far as drying of suspensions droplets is concerned, an explanation for the pattern formation due to deposition of particles at the periphery of a colloidal droplet (known as the coffee-ring effect) was first put forward by Deegan [13]. Numerous investigations have followed to understand the physicochemical dynamics of drying droplets [14-19]. Yunker et. al showed that the shape of the components present in a system influences the final pattern [20]. They found that the ring pattern formed in suspensions with spherical particles can be eliminated by use of ellipsoidal particles, where a more uniform deposition is obtained. The ring-type deposit in droplets of colloidal suspension can also be manipulated using proteins as shown by Devineau et. al [8]. Another work by Tsapis showed that a droplet placed on a hydrophobic substrate depicts a unique buckling instability which is absent on a hydrophilic substrate [21]. Therefore, it can be seen that the morphologies of dried out patterns is a complex interplay of several governing parameters, including evaporation, flow dynamics, inter-particle interactions and substrate chemistry, among others.

Patterns from complex solutions, such as bio-fluids, are far more complicated due to the presence of multiple components as well as phase transition such as sol-gel in the system [6]. Small changes in the solution composition lead to dramatic changes in their dried-out patterns. This necessitates a complete analysis of the effect of composition of biological fluids on the drying process. Biological fluids are usually modelled as a suspension of colloidal particles, mainly proteins and dissolved salts [21-25]. The distribution of the components during drying of such a multi-component fluid droplet is thought to be caused by the competing effects of diffusion and advection within the droplet leading to the final complex patterns [21, 26-27]. The final intricate structure consisting of salt crystals and peripheral protein deposits was observed experimentally by Yakhno [25]. Yakhno also revealed the dynamical changes leading to the final structures in a protein-salt droplet drying on a hydrophilic substrate [23]. However, different salt ions interact differently with proteins [28]. To the best of our knowledge, patterns developing because of the interaction of multiple salts with protein at different concentration have not yet been studied. This aspect is paramount in understanding the dry out of the more complex phenomenon of bio-fluids. In this paper, we report the deposition patterns in dehydrating droplets of protein-salt aqueous mixtures at different concentration of the components. We used bovine serum albumin (BSA) and we studied the crystallization of magnesium chloride ($MgCl_2$) and potassium chloride (KCl) salts in presence of BSA protein. The stability of a solution is determined by the nature of forces of interaction between the constituent particles. Addition of salt alters the interactive forces due to electrostatic screening effects and can lead to protein aggregation and precipitation [29-32]. Both the protein and the salt concentration therefore play a crucial role in determining the features of the final structure.

Eventually, we aim to develop an advanced bladder cancer test using deposition patterns. Examination of bladder cancer is a very painful invasive technique which is required to be performed multiple times due to its high recurrence rate [33-34]. It is hoped that pattern analysis could be implemented as an appropriate non-intrusive tool for initial diagnosis of the disease. This could potentially be extended to a wide range of health conditions. We have collected a considerable amount of data for the study of pattern formation using biological fluids (blood and urine) from cancer patients and control groups. The final dried-out patterns vary remarkably between the cancer patients and the healthy group in terms of (with respect to cracks, crystal shapes and sizes) [unpublished data]. The changes observed in the final patterns are expected to be due to differences in composition of the bio-fluids caused by the disease. Therefore, it is crucial to understand the drying process leading to such variation in morphologies. However, it is very difficult to distinguish the effect of each component present in a bio-fluid upon the pattern formation due to the complexity of the fluid. We intend to understand the influence of the basic components of blood plasma which consists of mostly protein and salt ions (sodium, potassium,

magnesium, calcium, chloride, and bicarbonate) upon the final patterns. We employed BSA due to its similarities with the human serum albumin. Moreover, the protein concentration (albumin-globulin ratio) has been previously identified as a blood-based biomarker for predicting the survival rates in bladder cancer patients [33-34]. The results in the current work show the effect of variation in protein composition upon the crystal growth and morphologies of the final patterns. We intend to understand the influence of the salt ions as well in the pattern formation and we used $MgCl_2$ and KCl as the potential salts for the current study as these have not been extensively studied. We understand that the exact pattern analysis would require a rigorous parametric study of the various components present in the bio-fluids in order to devise a diagnosis tool. However, the objective of the current work is to provide an initial understanding of the effect of the basic components present in a bio-fluid droplet. The findings from this investigation could pave the way to elucidating the fundamental underlying mechanisms in the dry out process and pattern formation from bio-droplets. Further experiments with the other components (usually found in the plasma) will be necessary to provide a more detailed understanding of the distinctive pattern formation.

EXPERIMENTAL SECTION

Solution preparation

Bovine Serum Albumin (BSA) was dissolved as received (Sigma Aldrich, UK) in deionized water and kept refrigerated overnight. The salts ($MgCl_2$ and KCl) were also dissolved in deionized water to be used as stock solutions. The experiments were performed in three sets, two to identify the effect of the individual salts with the protein and the final set with the mixture of the two salts and the protein. The fluids are marked as: (i) L_1 = BSA+$MgCl_2$; (ii) L_2 = BSA+KCl and (iii) L_3 = BSA+$MgCl_2$+KCl. The final composition of BSA in the solution [L_1 and L_2] was varied between 1-7% (by weight) and the salt was varied from 0.5-2% (by weight). The concentration of the different components in the current work are close to those present in bio-fluids (especially urine) and so the results are expected to have in-vivo relevance. The third set of experiments [L_3] was performed with 3% (by wt.) of BSA and 0.5% (by wt.) of the salts ($MgCl_2$+KCl). The concentration of the salt mixture (KCl+$MgCl_2$) [0.5 % wt.] is the physiological limit of the salt ion concentration. The two salts in L_3 were varied in the ratio [$MgCl_2$: KCl] of 1:1, 2:1, 3:1, 5:1 and 7:1 (although the final salt concentration in the solution was fixed at 0.5% wt.). The experimental road map is also represented in the Table 1. The net density of the mixtures (estimated using mixing law) varies in the range 0.96-0.97 g/cm^3. The capillary length [$l_{cap}=\left(\frac{\sigma}{\Delta\rho g}\right)^{0.5}$; where, σ is the surface tension of the droplet, $\Delta\rho$ is the density difference between the two fluids sharing the interface and g is the acceleration

due to gravity] is around 2.7 mm which is comparable to the diameter of the droplets (~ 3 mm) [35]. Therefore, the effects of gravity are unlikely to be significant and the droplet shapes can be approximated as spherical caps.

Set (i) F_1=BSA+$MgCl_2$		Set (ii) F_2=BSA+KCl		Set (iii) F_3=BSA+$MgCL_2$+KCl	
BSA (wt.%)	$MgCl_2$ (wt.%)	BSA (wt.%)	KCl (wt.%)	BSA (wt.%)	$MgCL_2$:KCl (0.5 wt.%)
1	0.5 1 2	1	0.5 1 2	3	1:1
3	0.5 1 2	3	0.5 1 2	3 3 3	2:1 3:1 5:1
7	0.5 1 2	7	0.5 1 2	3	7:1

Table 1: The set of experiments performed.

Experiments

Droplets of 2.7 (±0.3) µl volume were deposited on a substrate using an automatic dispenser [KRUSS drop shape analyser, DSA100] and left for drying at room temperature (24^0C-25^0C). The humidity level was monitored as 32-37% throughout the experiments. The variation of the relative humidity (~5%) and the ambient temperature throughout the experiments in the current study was reasonably low. Therefore, humidity and temperature are assumed constant in the experiments. We used glass slides (roughness of around 10-12 nm) as the substrate which results in an initial contact angle of around 50^0 (±3). The slides were washed using isopropanol and then blow-dried using air jet prior to the experiments to avoid any contamination. The droplets were back-illuminated using a white light source (shadowgraphy) and the droplet evaporation evolution was captured (side views) using a digital camera [MAKO G, Allied Vision Technologies] which was operated at 1 fps. The physical parameters of the droplets (contact angle, height and diameter) were measured, from the images captured, using Image J software. The reproducibility of the results was confirmed by repeating the experiments five times in each case under the same drying conditions. The morphology of the final deposits was captured using an optical microscope. The schematic of the experimental set-up is shown in Figure 1.

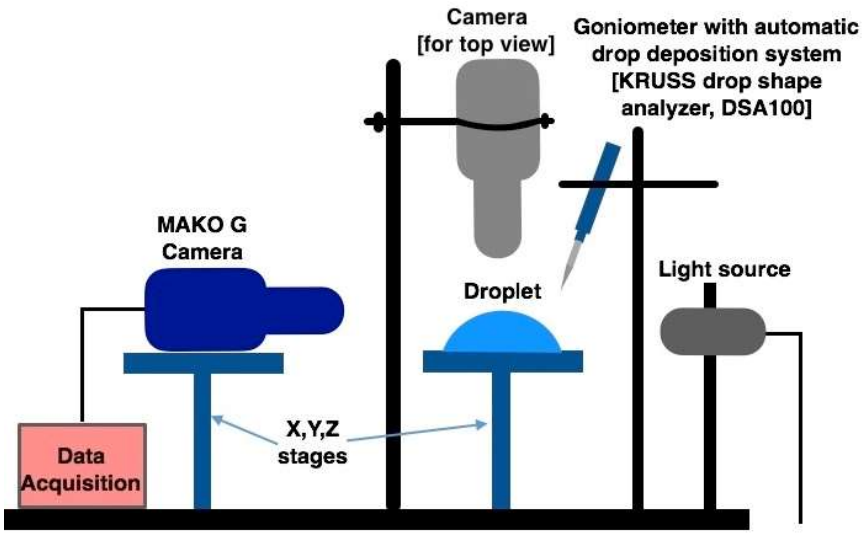

Figure1. Schematic of the experimental set-up.

RESULTS AND DISCUSSION

Pure protein droplets

A sessile colloidal droplet undergoes three dynamic stages during its lifetime. The first stage is the pure evaporation stage, which is similar to a pure fluid system (stage A, Figure 2(a)). The solute particles interact strongly with the substrate. The interactive van der Waals forces and the electrostatic interaction forces are evaluated as: $F_{VDW}=\frac{-2A}{3D^2}\frac{r^3}{(D+2r)^2}$ and $F_{Elec}=\kappa r Z e^{-\kappa D}$ respectively [where, A is the Hamaker constant between the particles, r is the particle size, D is the minimum separation distance, $\kappa^{-1}=\left(\frac{\varepsilon\varepsilon_0 k_B T}{\sum N_A I_i e^2 z_i^2}\right)^{0.5}$ is the Debye length and $Z=64\pi\varepsilon\varepsilon_0\left(\frac{k_B T}{e}\right)^2 \tanh\left(\frac{ze\psi_0}{4k_B T}\right)\tanh\left(\frac{ze\psi_S}{4k_B T}\right)$; ε and ε_0 are the dielectric constant and permittivity of free space respectively. k_B is the Boltzmann constant, T is the temperature, e is the electron charge, z is the surface charge, ψ_0 and ψ_S are the zeta potential of the particles and the substrate respectively] [29-30]. The protein-substrate interaction (~ $O(10^{-11})$ N) leads to the formation of a thin layer on the substrate at the centre of the drop which is smooth and featureless. The adhesion of proteins to the substrate causes a strong pining of the contact line of the drying droplets [36]. Therefore, motion of the contact line of a protein droplet is infinitesimally small throughout the droplet lifetime (constant contact radius mode of evaporation). The evaporation of liquid essentially causes a steady reduction in the contact angle of the droplet.

Additionally, for a sessile droplet placed on a hydrophilic substrate, the rate of evaporation is not uniform (it is higher at the edge of the droplet). This non-uniformity in evaporation leads to a radial

outward flow field inside the droplet driven by mass continuity. The internal flow imposes drag forces on the solute particles ($F_{drag}=6\pi\eta v$, r is particle radius, is the fluid viscosity and v is the flow velocity) which leads to deposition of the particles at the periphery of the droplet [13]. The drag force acting on the proteins in the current study is approximately of the order of ~ O (10^{-15}) N. The peripheral deposition of the protein is identified as a thick border of width d_b (stage B in Figure 2(b)). The width (d_b) increases with an increase in the initial concentration of protein in the droplet (Figure S1 in supplementary material). The stress build-up during evaporation is then released at the final stage of drying by the formation of periodic cracks on the surface of the deposit (stage C in Figure 2(c)). It is to be noted that the glass slides used in the current study are of similar chemical properties so that the consistency could be maintained throughout the experiments. It is therefore expected that the interaction between the glass substrate and the constituent particles will be consistent throughout the experiments and will only change with the change in composition of the droplets.

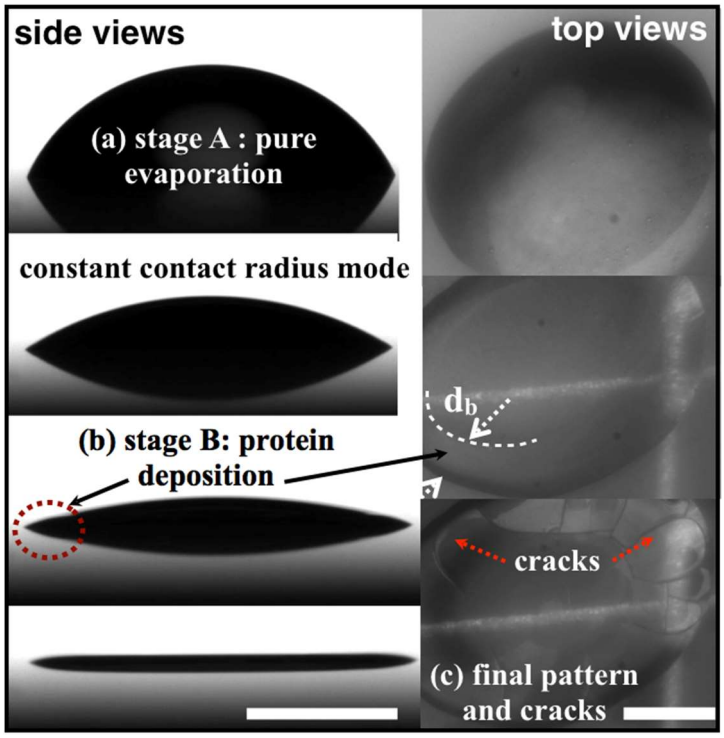

Figure 2. Different stages of drying in droplets of aqueous protein solution on a hydrophilic substrate [left panel: side views and right panel: top views; scale is 1 mm].

Protein droplets with added salts

The stability of a solution is determined by the nature of forces of interaction between the constituent particles which can be modelled by the DLVO (Derjaguin-Landau-Verwey-Overbeek) theory [29-30]. The van der Waals force of attraction and electrostatic repulsion forces are evaluated

as: $F_{VDW}=\frac{-A}{6D^2}\frac{r_1 r_2}{(r_1+r_2)}$ and $F_{Elec}=\kappa Ze^{-\kappa D}\frac{r_1 r_2}{(r_1+r_2)}$ respectively. Addition of salt alters the interactive forces due to electrostatic screening effects and can lead to protein aggregation and precipitation [30, 32]. Although the salts enhance both the forces of attraction (F_{VDW}) and repulsion (F_{Elec}), the force of attraction is higher than the repulsive forces. Therefore, the increase in particle-particle attraction is dominant over the repulsive interactions and leads to subsequent aggregation of the protein. It is also found that the net particle-particle interaction force is higher for KCl as compared to $MgCl_2$ (which is more prominent at higher salt concentration) (see supplementary material). The higher ionic strength of $MgCl_2$ solution (I for $MgCl_2$ is three times that of KCl at 2% wt.) could lead to lower net interaction forces. However, the evaluation of the exact behaviour would require comprehensive estimation of the particle-particle interactions (which is beyond the scope of this work).

In droplets with added salts, the protein deposit may act as a nucleation point for the crystallization of the salts. The drag force (F_{drag}) experienced by the protein particles is slightly greater than that of the salt (15%) which leads to earlier deposition of protein at the periphery and subsequent deposition of the salt at the inner periphery of the protein ring. This leads to a multiple-ring type pattern. The loss of solvent and depletion of protein from the inner region increases the local concentration of salt in the droplet and eventually crystallization is initiated as the salt concentration exceeds the saturation limit. It should be noted that the drag force reduces significantly (by two orders) prior to the initiation of crystallization and is expected to have no contribution in the growth of the crystals. Alternatively, the solvent evaporation causes a reduction in the separation distance between the particles (D) and leads to a significant rise in the particle-particle interactions. For instance, the van der Waals force of attraction is increased by 2.5 times during crystallization although the electrostatic forces (F_{elec}) changes by only 7% (see Figure S3 in the supplementary material). Therefore, the particle-particle interaction plays a crucial role in the process of crystallization while the drag forces only assist in the initial organization of the constituent particles in the droplet.

The interpretation of salt and protein structures in the final pattern is critical as the pattern alters significantly, even for a slight change in the concentration of any one component in the mixture. The results of salt-protein droplet drying will be shown and explained in the following sections.

Results of BSA + $MgCl_2$ droplets

Figure 3 shows enlarged images of the final deposits of nine droplets of different BSA and $MgCl_2$ composition with the concentrations of BSA and $MgCl_2$ on the X-axis and Y-axis respectively. It is

to be noted that a droplet of pure aqueous solution of $MgCl_2$ does not dry due to its hygroscopic behavior and hence no crystallization was observed for it even after a week's time. Interestingly, in the presence of BSA (1% wt.), $MgCl_2$ forms crystals of different shapes (average length, l_{crys} ~ 20−40 μm) which remain uniformly deposited throughout the surface area (type (i) in Figure 3a). The crystals are not noticeable at the periphery of the deposited pattern. The crystals formed (if any) might have been overshadowed by the thick deposit of protein at the periphery and hence are not detected in the microscopic images. As stated earlier, a dehydrating protein droplet (in absence of any salt) forms a uniform deposit on the substrate with a number of cracks on the surface that appear to propagate radially (Figure 2c). However, with salt present, the protein in the droplet helps in dehydration, which assists in crystallization of the $MgCl_2$ salt. Surprisingly, the type (i) crystals are not observed at higher concentration of the salt (1% wt.-2% wt.) in the droplet. The amount of protein (1% wt.) present in the droplet may not be sufficient to induce salt crystallization in the droplets with higher salt concentration (1% wt.-2% wt.). A small number of salt aggregates (type (ii)) are deposited in the final pattern at 1% wt. $MgCl_2$ concentration. This may be due to incomplete crystallization of the salt due to its hygroscopic nature. We observed that the hygroscopic nature of $MgCl_2$ becomes dominant above a certain threshold value (≥ 1% wt.) due to insufficient protein (1% wt.) in the droplet. This results in a large number of tiny crystals ($O(10^{-3})$ mm) which remain deposited in the central region of the droplets. The quantity of these smaller crystals increases (by two times) with further increase in the salt concentration (2% by wt.). The small crystals could be salt particles which remain trapped in the protein layer deposited on the substrate and did not undergo any further crystallization. These trapped particles only become perceptible at the end of the droplet lifetime due to complete evaporation of the solvent.

An increase in the concentration of BSA (3% wt.) enhances the growth of the salt crystals. A number of isolated crystals (single blocks) are formed at 0.5% wt. concentration of $MgCl_2$ (type (iii) in Figure 3b). The type (iii) crystals are also observed at 1% wt. of $MgCl_2$. However, the higher amount of salt (1% wt.) in the droplet results in aggregation of these type (iii) crystals. The peripheral thickness of the protein deposit (d_b in Figure 2) is increased with an increase in the protein concentration (d_b ~ 0.2 mm and 0.6 mm for 1% BSA and 7% BSA respectively). The initial contact area is similar across various composition (contact diameter ~ 3 mm, contact angle ~ 50^0). Therefore, the area available for the salt crystals (central region) is reduced with an increased amount of protein in the droplet due to the formation of a thicker periphery (evident as an increase in d_b). The spatial restriction and continuous solvent evaporation leads to the aggregates of type (iii) crystals at higher salt concentration (1% wt. $MgCl_2$). Formation of crystals is completely suppressed at 2% wt. $MgCl_2$ due to insufficient protein and lumped deposits of the salt (type (ii)) are observed in the final pattern.

Interestingly, further increase in the concentration of BSA (7% wt.) causes a transition to chains of crystals (aspect ratio of 10) at 0.5 wt. % of $MgCl_2$ (type (iv) in Figure 3c). Higher concentration of protein enhances the rate of evaporation of the solvent in the droplet [$t_{evap} \sim$ 800 s and 1200 s at 7% wt. and 1% wt. of BSA respectively (see Figure S5 in the supplementary material)]. Absorption of water by protein lowers the surface tension of the droplets which increases the exposed surface area and this could lead to higher evaporation rates at higher protein concentration. Faster drying leads to the formation of elongated crystals which do not show any preferential alignment and are randomly distributed throughout the droplet deposit. The local concentration gradients could possibly lead to such random orientation. The transition of crystal shapes from type (i) to type (iv) is also observed at higher concentration of the salt (1% wt.). This indicates that an optimum amount of protein (> 3% wt.) is required to form the chains of crystals. However, the chain-type crystals are absent at higher concentration of $MgCl_2$ (2% wt.) and lumped deposits of salt (type (ii)) are formed in the central region of the final pattern. It can thus be inferred that the chain-type arrangement of crystals can be achieved only up to a maximum concentration of the salt (around 1% wt.). The upper limit of the salt crystallization appears to be determined by the initial concentration of the salt relative to the protein in the droplet. Therefore, an optimum amount of both protein and salt determines the characteristics of the crystals in $MgCl_2$+BSA droplets. An excess of salt is always deposited as a lumped mass (type (ii)) in the final pattern, irrespective of the protein concentration. The particle-particle interaction forces might play a crucial role in in crystallization. For instance, the net DLVO forces ($F_{net}=F_{VDW}+F_{Elec}$) are enhanced (by almost two times) with an increase in salt concentration (2% wt.) and these forces might hinder the formation of chain-type crystals at higher salt concentration (2% wt. $MgCl_2$) (see Figure S2 in the supplementary material).

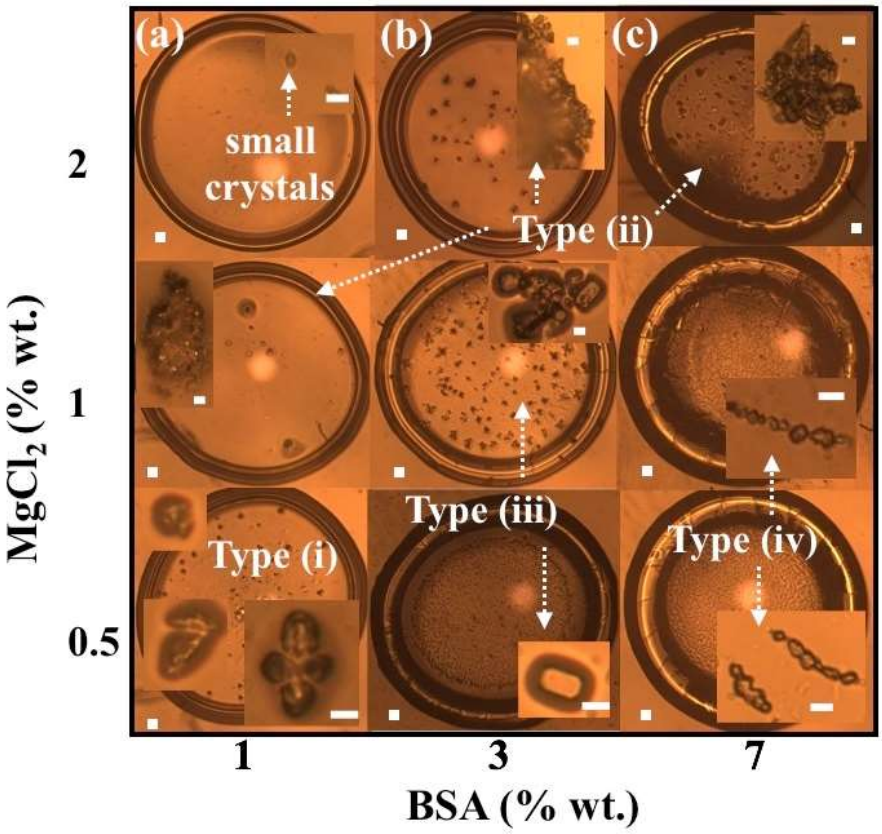

Figure 3. The different types of patterns obtained at different concentration of $MgCl_2$ + BSA droplets [concentration of BSA and $MgCl_2$ are placed on X-axis and Y-axis respectively] [scales represent 0.1 mm for the enlarged images and 5 µm for the inset images respectively].

Results of BSA + KCl droplets

Figure 4 depicts the final patterns formed due to drying of BSA+KCl droplets of nine different compositions. The concentrations (in % wt.) of the components (BSA and KCl) are plotted on the X-axis and Y-axis respectively. KCl tends to form regular rectangular-shaped crystals (~ O (10^2) µm) at 1% wt. of BSA solution [inset: Figure 4 (left panel)]. Pure evaporation (Stage A) occurs for around 90-95% of the droplet lifetime (t_{evap} ~ 90-95% t_{life}) and leads to the deposition of protein as stated earlier (radial thickness, d_b ~ 0.1 mm) (Figure 5a). The thickness of the protein deposit (d_b) is similar across various concentrations of KCl (0.5-2 % wt. not shown here) which suggests that the salt has no impact upon the protein deposition. It should be noted that the thickness observed in the final patterns (Figure 4) is the apparent thickness (d_f) due to the growth of the salt crystals and not the protein rim thickness (d_b). The crystals deposited at the periphery cause a three-fold increase in the apparent thickness of the protein layer (d_f ~ 0.3 mm) at the end of the drying process. The deposits of BSA appear to act as nucleation points for the salt. The crystallization is initiated at several points (simultaneously) at the peripheral protein deposit when the saturation concentration of the salt (58 g/100 g of water [37]) is exceeded (Figure 5b). It is seen that the droplet volume reduces to about 0.1-0.2 µl at the point of initiation of the crystallization. At this point, the

concentration of the salt is estimated to be around 20-25 % by wt. (depending upon the initial compositions), which is less than the saturation concentration (37% by wt.). It is to be noted that the components are assumed to be uniformly distributed within the droplet. However, the salt concentration might exceed the saturation limit locally which leads to crystallization. This is evident as the crystallization is initiated at random points at the periphery and within the central region of the droplet (Figure 5b). The peripheral crystals are of different shapes (average length-scale, $l_{avg} \sim 0.2$ mm) which grow radially at a rate of $\left[\frac{dl_{crys,peri}}{dt_{crys}}\right] \sim 0.01$ mms^{-1}.

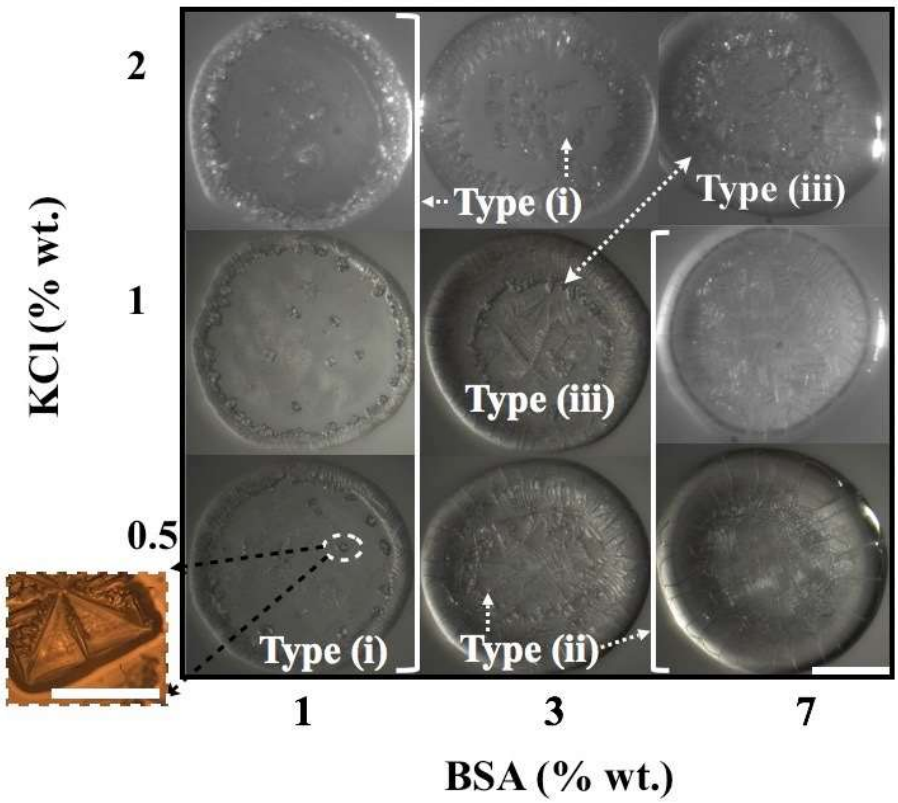

Figure 4. The different types of patterns obtained in KCl+BSA droplets [concentration of BSA and KCl are placed on X-axis and Y-axis respectively] [scale represents 0.1 mm].

The crystals in the central region of the droplet are more rectangular (length, $l_{crys} \sim 0.2$ mm and width, $w_{crys} \sim 0.05$ mm), which is typical of pure KCl crystallization. Formation of these crystals causes depletion of solution around them [5]. Spatial confinement and continual evaporation of the liquid phase leads to the formation of small crystals (1-20 μm) covering the entire deposited area (Figure 5d). The water trapped between these crystals eventually evaporates and leads to dendritic growth of crystals ($w_{crys} \sim 0.001$ mm). These dendritic crystals progress with branching (at an angle of 80±10 degrees) towards the periphery of the deposit (Figure 5d). The growth rate of the dendritic

crystals $\left[\frac{dl_{crys,dendrites}}{dt_{crys}} \sim 0.07\ mms^{-1}\right]$ is faster than that of the peripheral crystals. This droplet pattern is termed as type (i) (Figure 4). The pattern (type (i)) is consistent across various concentration of the salt (0.5-2 % wt.) in 1% (by wt.) BSA solution (Figure 4). The rate of crystallization is also consistent at different salt concentration. However, the total timescale of crystallization (peripheral + dendritic crystals) (Stage B) is enhanced (by about five times) for a four-fold increase in the salt concentration [$t_{crys} \sim 100$ s for 2% KCl]. The number of crystals deposited at the periphery also increases at higher salt concentration.

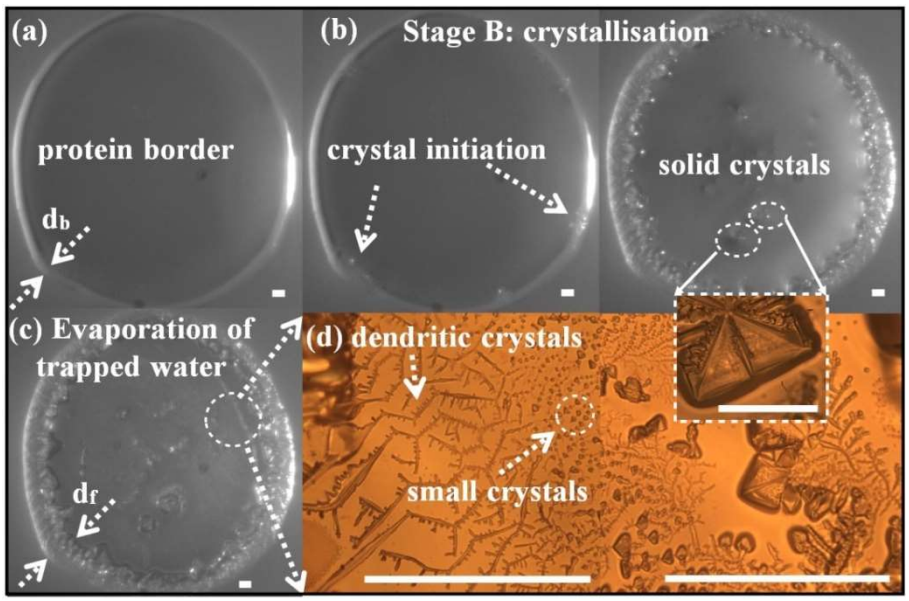

Figure 5. The various stages of crystallization in type (i) pattern obtained in BSA+KCl droplets (the images are for: 1% wt. BSA+2% wt. KCl) [scale represents 0.1 mm].

The rate of evaporation (Stage A) is estimated as the reduction in droplet volume (2.5×10^{-12} m^3/s) and the rate increases by only 20% for an increase in the salt concentration by two times (Figure 6). The variation in the evaporation rates could be due to the complex interaction of salt ions with protein. The crystallization of salts might create local air-liquid interfaces which are unstable and could possibly lead to higher evaporation rate at higher salt concentration [38]. However, we cannot explain the evaporation dynamics in detail with the current experimental work. As stated earlier, the flow induced by evaporation only leads to an initial distribution of particles in the droplet prior to the crystallization. The increase in timescale of crystallization with an increased salt concentration is caused solely due to higher amount of salt present in the droplet and not due to variation in the evaporation rate. It should be noted that the volume is measured up to the point when no further change is detected in the images. The volume might still be decreasing but the rate is extremely

small (~O(10^{-15}) m^3/s) as compared to the earlier stages and hence not considered in the calculations.

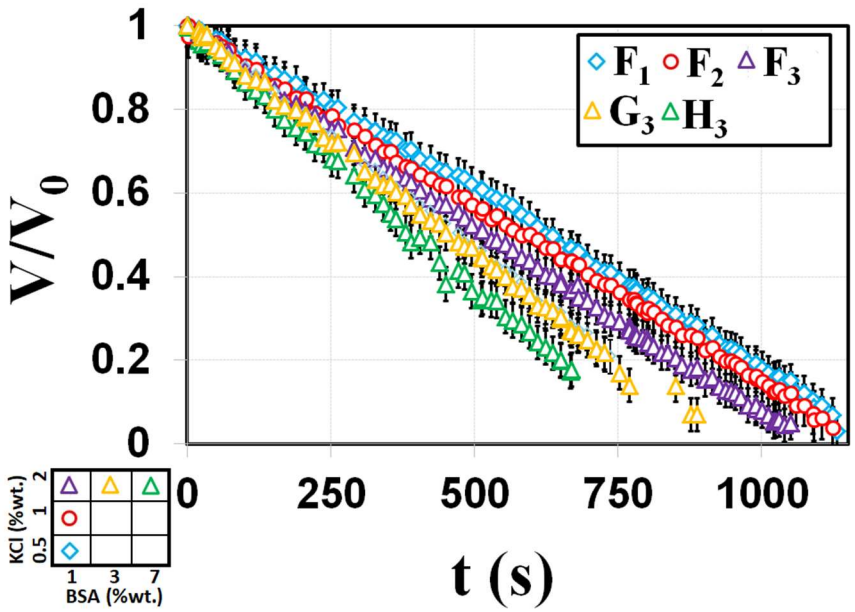

Figure 6. Temporal variation of droplet volume (V), non-dimensionalized with the initial droplet volume (V_0), at various concentration of KCl and BSA [F_1: 1% wt. BSA+0.5% wt. KCl; F_2: 1% wt. BSA+1% wt. KCl; F_3: 1% wt. BSA+2% wt. KCl; G_3: 3% wt. BSA+2% wt. KCl; H_3: 7% wt. BSA+2% wt. KCl; (volumetric reduction is not plotted for some fluids (G_1,G_2, H_1 and H_2) to maintain clarity of the figure, otherwise the graphs follow similar trend as the fluid F_1, F_2 and F_3] [deviation from mean graph is around ±5%].

An increase in the concentration of BSA to 3% (by wt.) causes significant alteration in the pattern of crystallization. The regular (rectangular shaped) crystals of the salt are not observed in these droplet patterns. Higher amount of BSA induces vigorous dendritic growth of crystals for 0.5% wt. of KCl (Figure 4). The dendritic crystals originate at the periphery and in the central region simultaneously (Figure 7b). These crystals undergo radial growth with branches (w_{crys} ~ 0.01 mm) at 90 degrees angle to the main crystal stem. The dendritic roots then extend over the peripheral protein deposits (Figure 7c). This highly dense dendritic pattern is represented as type (ii) (Figure 4). It should be noted that the growth rate of the dendrites $\left[\frac{dl_{crys,dendrites}}{dt_{crys}} \sim O\left(10^{-1}\right) \text{ mms}^{-1}\right]$ is higher than that of the dendrites at 1% BSA (Figure 8). Previously, the dendritic crystal structure was attributed to faster drying and spatial constraint [39]. In the current experiments, the rate of solvent evaporation increases (by only 30%) at 3% wt. BSA (10^{-3} µl/s) during stage A (pure evaporation) (Figure 6). However, the evaporation rates could be estimated from the side view imaging only

prior to the initiation of crystallization (stage B) due to experimental limitations. The rate of evaporation of trapped water (following stage A) might be even faster at higher protein concentration which leads to faster dendritic growth at 3% wt. BSA. It should be noted that the dendrites in the type (ii) pattern are different from the dendrites in the type (i) patterns. The difference is evident in the size of the dendrites which is an order of magnitude larger at 3% wt. BSA (width, $w_{crys} \sim 0.01$ mm). Additionally, the dendrites formed at 3% wt. BSA are more stable (less splitting) (Figure 7) while those at 1% BSA are formed with highly splitting ends (Figure 5d).

Loss of solvent due to evaporation causes precipitation of protein which covers the surface of the salts [39]. Two more unstable moving interface are formed, one between protein-salt (σ_{ps}) which is more anisotropic and another between protein-liquid (σ_{pl}) which is more isotropic in nature [39]. The crystals formed after drying of pure aqueous KCl solution droplets are of cubic shape (see Figure S6 in the supplementary material). The presence of protein reduces the anisotropy (due to isotropic nature of σ_{pl}) and leads to fractal growth of KCl crystals. Addition of salts enhances the surface tension of the air-water interface (σ_{aw}). However, the increase in air-liquid interfacial tension due to addition of salt is expected to have a similar effect across the various concentration of the salt (0.5% wt. to 2% wt.).

The dendritic growth of KCl crystals is also observed at a protein concentration of 7% wt. (type (ii) in Figure 4) up to a salt concentration $\leq$ 1% wt. This elucidates the fact that a threshold concentration of protein ($\geq$ 1% wt. BSA.) is required for the dendritic pattern of crystallization (type (ii) pattern). The smaller dendrites formed at 1% wt. BSA (towards the end of Stage B) are solely due to spatial restriction and faster evaporation of the trapped residual water (as explained earlier) although the threshold BSA concentration is not attained. Increase of salt concentration to 1% (wt.) leads to another interesting type of pattern at 3% wt. BSA concentration (termed as type (iii) in Figure 4). The crystallization is initiated at the periphery with the formation of elongated crystals (Figure 9). These crystals grow radially inward ($l_{crys} \sim 0.3$ mm) at a rate of $\left[\frac{dl_{crys,peri}}{dt_{crys}} \sim 0.06 \text{ mms}^{-1}\right]$ and are followed by the development of dendritic crystals in the central region. These dendrites in the central region extend radially outward towards the periphery. The final pattern is an intermediate between type (i) and type (ii) patterns as it consists of both the regular (elongated) crystals (at the periphery) and dendritic crystals (in the central region) (type (iii) in Figure 4).

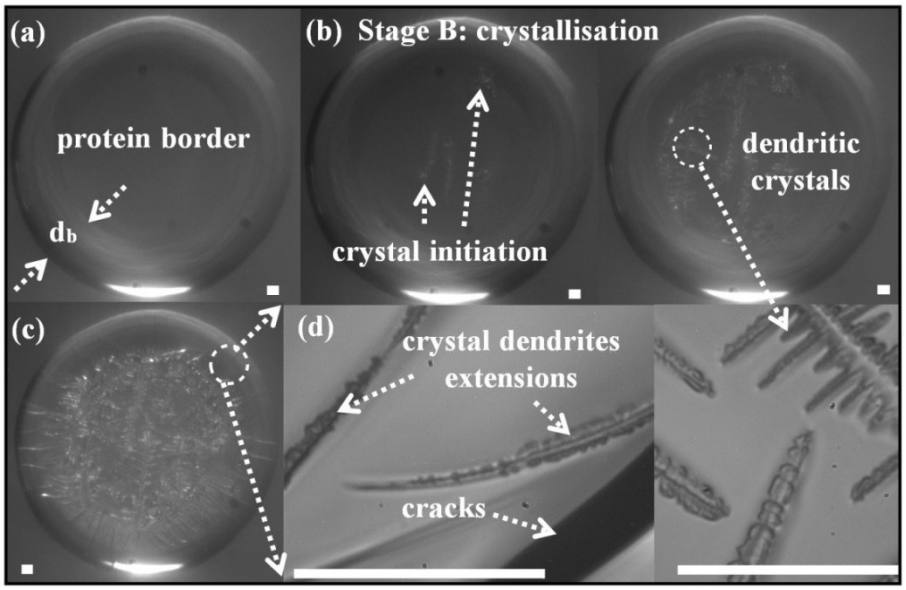

Figure 7. The various stages of crystallization in type (ii) pattern obtained in BSA+KCl droplets (the images are for 7% wt. BSA+0.5% wt. KCl) [scale represents 0.1 mm].

Evaporation leads to a concentration gradient within the droplet. Therefore, the crystal grows due to mass diffusion led by the concentration gradient and the rate of growth can be scaled as: $v_{crys} \sim D/l$ [D is the mass diffusivity of KCl and l is the diffusion lengthscale]. The diffusion lengthscale "l" can be scaled as: $l \sim \sqrt{A}$ (where, $A = A_{drop} - A_{protein} - nA_{crys}$, is the total surface area available for the growth of the dendritic crystals in the deposit; A_{drop} and $A_{protein}$ are the surface areas of the dried out droplet and the peripheral protein deposit respectively. A_{crys} is the average area of the total (n) number of rectangular crystals (if any) already formed in the central region of the deposit). The protein deposits formed at the periphery ($A_{protein}$) reduces the space available for the growth of the dendritic crystals. This is evident as the periphery is thicker due to high protein deposition (radial thickness, $d_b \sim 0.5$ mm at 7% wt. BSA). Therefore, diffusion lengthscale (l) is significantly reduced which enhances the rate of crystallization (v_{crys}) at higher protein concentration (Figure 8). However, the slower growth rate of the dendritic crystals in pattern type (iii) even at higher protein concentration ($\geq$ 3% wt.) cannot be explained using the diffusive lengthscale. The diffusivity (D) of the salt might be influenced by the presence of protein in the droplet and this may lead to such slower growth rates. The variation of diffusivity (D) with the protein concentration has to be incorporated for the exact calculation of v_{crys}. It should be mentioned here that the influence of flow field inside the droplet is not considered in the calculation. It is justified as the velocity induced due to evaporation (v_{evap}) is estimated to be of the order of $\sim O(10^{-4})$ mms^{-1} which is 2-3 orders less than the crystal growth rates at any composition ($v_{crys} \sim O(10^{-2}\text{-}10^{-1})$ mms^{-1}. Here, v_{evap} is estimated using the global evaporation rate $\left(\frac{dV_{drop}}{dt} = \frac{\pi}{2}\left(d^2 + h^2\right)v_{evap}\right)$, by assuming a spherical cap with a fixed

contact diameter (d) and varying height (h) (where, V_{drop} is the volume of the droplet).

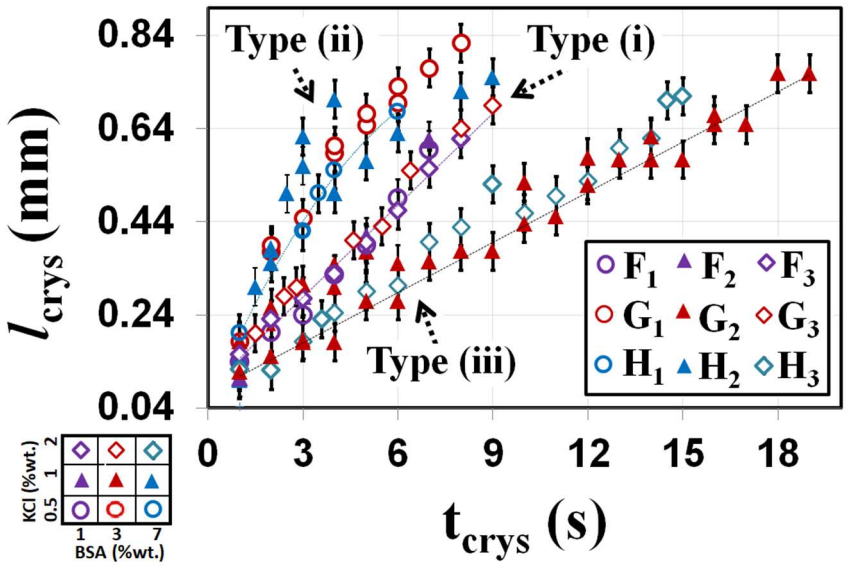

Figure 8. Temporal variation of average size of the dendritic crystals obtained in the dried-out patterns of BSA+KCl droplets [F_1: 1% wt. BSA+0.5% wt. KCl; F_2: 1% wt. BSA+1% wt. KCl; F_3: 1% wt. BSA+2% wt. KCl; G_1: 3% wt. BSA+0.5% wt. KCl; G_2:3% wt. BSA+1% wt. KCl; G_3: 3% wt. BSA+2% wt. KCl; H_1: 7% wt. BSA+0.5% wt. KCl; H_2: 7% wt. BSA+1% wt. KCl; H_3: 7% wt. BSA+2% wt. KCl] [deviation from the mean graphs are around 5-7% for the different fluid systems].

The dendritic growth is completely suppressed at higher concentration of KCl (2% wt.). Interestingly, the pattern formed consists of regular crystals in the central region similar to type (i) at 3% wt. BSA and the peripheral deposits of elongated salt crystals similar to the transition patterns (type (iii)) at 7% wt. BSA (Figure 4). We can still consider these as type (i) patterns. It adds credence to the conjecture that an optimum amount of BSA relative to the salt concentration is required for the dendritic growth of crystals (type (ii) and type (iii)). The condition of optimum concentration of the components to form the desired crystals was also observed in $MgCl_2$ added protein droplets (section 3.1).

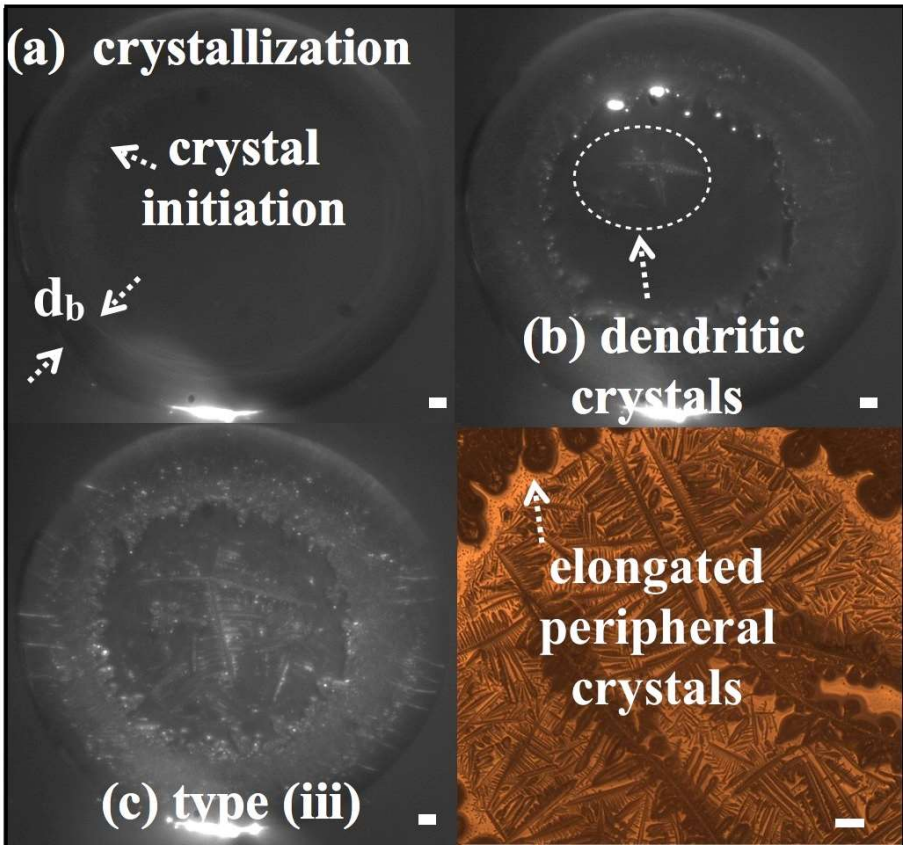

Figure 9. The various stages of crystallization in type (iii) pattern obtained in BSA+KCl (the images are for: 3% wt. BSA+1% wt. KCl) [scale represents 0.1 mm].

It should be noted that the final (average) size of the peripheral crystals (l_{crys}) are uniform across various salt concentration (0.5-2 % wt. KCl) and varies only with a variation in the protein concentration (1-7 % wt.). These crystals nucleate solely due to the protein deposits. Therefore, the crystal growth is governed by the amount of protein available in the droplet. This is evident by plotting the temporal variation of the average size of the crystals (l_{crys}) which is non-dimensionalized using the width of the peripheral protein deposit (d_b) (Figure 10). The time for crystal growth (t_{crys}) is non-dimensionalized with the the total time for crystallization (t_{tot}) [t_{tot} is calculated from the point of initiation of the crystals to the point where no change in the size of the crystals was observed]. The protein is deposited uniformly upon the substrate and the peripheral width (d_b) varies depending upon the initial protein concentration in the droplet. Therefore, the peripheral protein deposit (d_b) is considered as a suitable scale for non-dimensionalization of the peripheral crystals. The temporal variation of "l_{crys}/d_b" is uniform across various concentration of the two components (BSA and KCl). It is to be noted that the peripheral crystals are either absent or indistinguishable due to densely formed dendritic structures in type (ii) patterns (fluid system G_1, H_1 and H_2) and hence not plotted in the Figure 10.

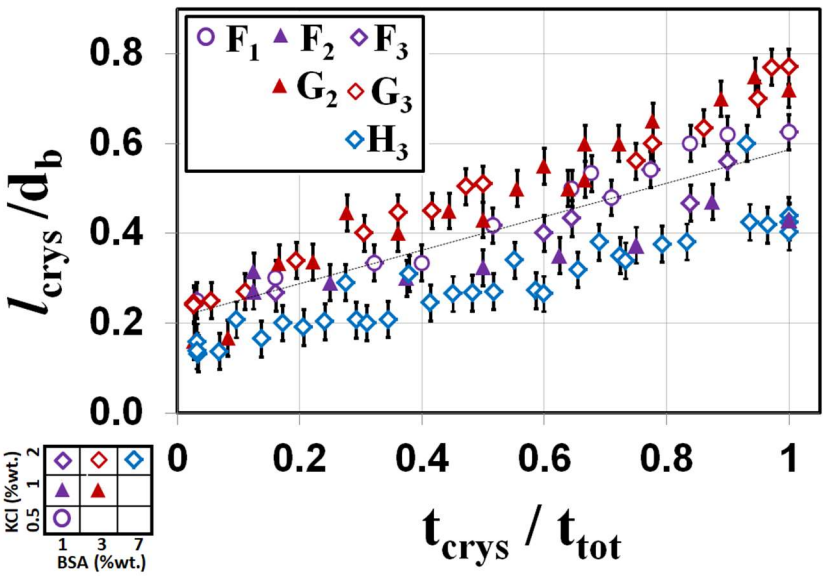

Figure 10. Temporal variation of average size of the peripheral crystals (l_{crys}) obtained in the dried-out patterns of BSA+KCl droplets [F_1: 0.5% wt. KCl+1% wt. BSA; F_2: 1% wt. KCl+1% wt. BSA; F_3: 2% wt. KCl+1% wt. BSA; G_2: 1% wt. KCl+3% wt. BSA; G_3: 2% wt. KCl+3% wt. BSA; H_3: 2% wt. KCl+7% wt. BSA].

Results of BSA + mixed salt ($MgCl_2$+ KCl) droplets

The final set of experiment was performed with mixed salts ($MgCl_2$ and KCl) in BSA (3% by wt.) and the final patterns are shown in Figure 11. The total concentration of salts was fixed at 0.5% wt. The composition of the salts was varied in the ratio of ($MgCl_2$: KCl) 1:1, 2:1, 3:1, 5:1 and 7:1. The droplets with equal concentration of the two salts [$MgCl_2$:KCl = 1:1] shows dendritic growth of crystals originating in the central region (Figure 11). The pattern is similar to type (ii) observed in BSA+KCl droplets with a composition of 3% (wt.) BSA and 0.5% (wt.) KCl (Figure 4) with an equivalent growth rate $\left[\frac{dl_{crys}}{dt_{crys}} \sim O\left(10^{-1}\right) \text{ mms}^{-1}\right]$. The timescale of crystallization is also similar ($t_{crys} \sim$ 25 s) to BSA+KCl droplets, which reveals the dominant nature of KCl over $MgCl_2$ even for equal concentration of the salts (1:1). The timescale of crystallization for $MgCl_2$ in presence of BSA (L_1) is about an order of magnitude higher than that of KCl in BSA (L_2) for a similar concentration. Therefore, the crystals observed in the final pattern of mixed salt droplets (L_3) are believed to be formed mostly of KCl.

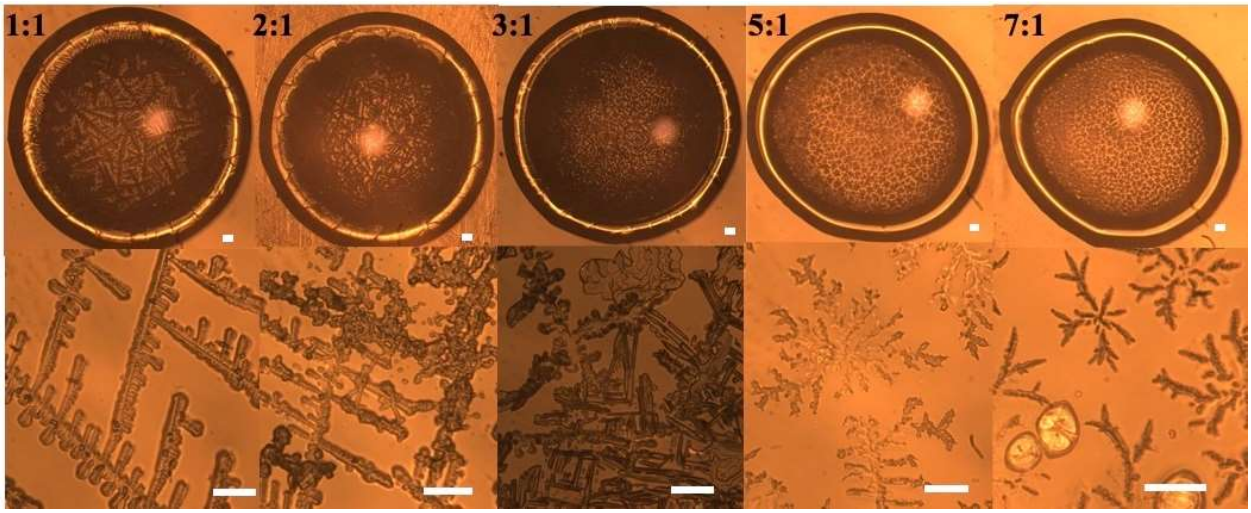

Figure 11. The final patterns obtained in droplets of BSA+mixed salts ($MgCl_2$+KCl) [scale represents 0.1 mm (top row) and 20 microns (bottom row)].

An increase in the amount of $MgCl_2$ leads to a destruction in the regularity of the arrangement of the dendritic crystals in the pattern. The dendritic arrangement is completely eradicated above a threshold composition of 3:1. Further increase in $MgCl_2$ (5:1) leads to the formation of snow-flake-shaped crystals with dendritic ends (branches of 1 µm thick). The thickness of the branches reduces by 50% (0.5 µm) at the composition of 7:1. Increasing the concentration of $MgCl_2$ causes a simultaneous reduction in the absolute amount of KCl in the droplet. Reduction of KCl concentration (by two times) reduces the rate of solvent evaporation in the droplet (by 20%) as was observed in KCl+BSA droplets (Figure 6).

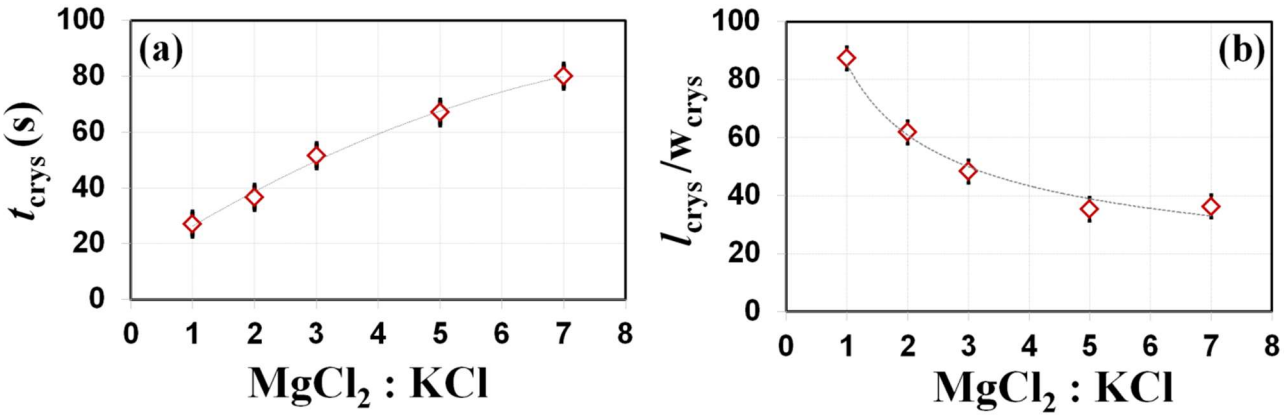

Figure 12 (a) Variation of time required for crystallization (t_{crys}) in the droplets of BSA+$MgCL_2$+KCl (concentration of BSA and salt mixture ($MgCL_2$+KCl) are 3% wt. and 0.5 % wt. respectively) [deviation from mean graph is around ±6 %] and (b) variation of the aspect ratio (l_{crys}/w_{crys}) of the crystals in the droplets of BSA+$MgCl_2$+KCl (concentration of BSA and salt

mixture ($MgCl_2$+KCl) are 3% wt. and 0.5 % wt. respectively) [deviation from mean graph is around 6 %].

Alternatively, increase in $MgCl_2$ concentration (by two times) enhances the evaporation rate (by about 11%) as was observed in $MgCl_2$+BSA droplets (not shown here). It should be noted that the change in the ratio of the two salts ($MgCl_2$:KCl) from 1:1 to beyond the transition ratio 3:1 is equivalent to a reduction of the absolute amount of KCl by about two times and a similar increase in the amount of $MgCl_2$. Therefore, the evaporation rate is defined by a competitive effect of both the salts. The evaporation rate is measured as the volumetric size reduction of the droplets [$(dV_{drop}/dt) \sim O(10^{-3})$ mm^3s^{-1}]. The net effect results in a slow crystallization [by about three times] (Figure 12a) and prevents the dendritic growth of crystals (Figure 12b). The mass diffusivity of $MgCl_2$ is twice that of KCl in aqueous solution ($D \sim 10^{-9}$ m^2 /s) [40-41]. The net diffusion rate of the salts might be reduced at higher concentration of $MgCl_2$, which also contributes in the reduced rate of crystallization. However, a detailed study of the instabilities leading to the variations in the final patterns observed in the current work is required for a complete understanding of bio-fluid droplets. Further investigation on some of the instabilities driving the system will be performed in future work.

SUMMARY AND CONCLUSIONS

We have experimentally investigated the different types of patterns formed due to dehydrating protein-salt droplets on hydrophilic substrates (glass). We incorporated two salts ($MgCl_2$ and KCl; individually and combined) in an aqueous protein solution (Bovine Serum albumin, BSA). The influence of protein in the crystallization of salts is observed in both $MgCl_2$ and KCl. $MgCl_2$ + BSA forms four different types of patterns (consisting of crystals of irregular shapes, single blocks and crystal-chains) depending upon the initial concentration of the two components. The crystallization of $MgCl_2$ is enhanced in the presence of protein although an excess amount of salt is always deposited as a lumped mass in the pattern. KCl in BSA leads to the formation of three different types of patterns (consisting of block crystals, dendritic crystals and peripheral crystals respectively). Interestingly, all these patterns can be modulated by controlling the initial concentration of the components in the droplet. Differential diffusion rate of the components can lead to drastic changes in the final patterns. In addition, the local drying of trapped solvent also defines the microscopic features (especially dendritic crystals) in the pattern. Finally, we studied the dried-out patterns of combined salts ($MgCl_2$+KCl) in BSA. We found that the ratio of the two salts plays an important role in determining the features of the final pattern. The effects of KCl (leading

to dendritic crystals) is dominant over $MgCl_2$ upto a threshold concentration (which is $MgCl_2$: KCl = 3:1), beyond which the effect of $MgCl_2$ becomes more prominent, leading to the formation of snow-flake type crystals in the patterns. The work can be summarized as a parametric study of the consequences of varying droplet composition upon the final dried-out structures. The results of this study provide useful insights into the mechanisms underlying the formation of patterns in complex solutions like biofluids. These findings provide a preliminary understanding of the differences observed in the dried out patterns of bio-fluid droplets (blood and urine) of patients and healthy controls. Further investigations using different compositions will be necessary to implement pattern analysis as a tool for diagnosis of bladder cancer and will be performed in our future work.

ASSOCIATED CONTENT

Supporting information

SM1: Sped up video clip (MP4) of the side view of an aqueous BSA droplet evaporating as reported in Figure 2

SM2: Sped up video clip (MP4) of the top view of an aqueous BSA droplet evaporating as reported in Figure 2

SM3: Sped up video clip (MP4) of the top view of an aqueous 1% wt. BSA+2% wt. KCl droplet evaporating as reported in Figure 5

SM4: Sped up video clip (MP4) of the top view of an aqueous 7% wt. BSA+0.5% wt. KCl droplet evaporating as reported in Figure 7

SM5: Sped up video clip (MP4) of the top view of an aqueous 3% wt. BSA+1% wt. KCl droplet evaporating as reported in Figure 9

SM6: Additional figures:
Figure S1. Final deposit of BSA droplets
Figure S2. Comparison of the net DLVO forces
Figure S3. Temporal variation of different intermolecular forces
Figure S4. Variation of DLVO forces with salt concentration
Figure S5. Temporal variation of droplet volume
Figure S6. Final deposit of KCl crystals
Figure S7: Estimation of l_{crys}.

AUTHOR INFORMATION

Corresponding Author

*E-mail: J.Christy@ed.ac.uk . Phone: +44(0) 131 6504854

ACKNOWLEDGEMENTS

We gratefully acknowledge the financial support received from the Katip Celebi Newton Fund.

REFERENCES

[1] Reynaud, E., Protein misfolding and degenerative diseases. *Nature Education* **2010**, *3*(9), 1-28.

[2] Kastelic, M., Kalyuzhnyi, Y.V., Hribar-Lee, B., Dill, K.A. and Vlachy, V., Protein aggregation in salt solutions. *Proceedings of the National Academy of Sciences* **2015**, *112*(21), 6766-6770.

[3] Shabalin, V. N.; Shatokhina, S. N., Diagnostic markers in the structures of human biological liquids. *Singap. Med. J.* **2007**, *48*, 440–446.

[4] Martusevich, A. K.; Zimin, Y; Bochkareva, A., Morphology of dried blood serum specimens of viral hepatitis. *Hepatitis Mon*. **2007**, *7*, 207–210.

[5] Yakhno, T. A., Complex pattern formation in sessile droplets of protein-salt solutions with low protein content. What substance fabricates these patterns. *Phys. Chem.* **2011**, *1*(1), 10-13.

[6] Rapis E., A change in the physical state of a non-equilibrium blood plasma protein film in patients with carcinoma. *Technical Physics* **2002**, *47*, 510–512.

[7] Brutin, D.; Sobac, B.; Loquet, B.; Sampol, J. Pattern formation in drying drops of blood. *Journal of fluid mechanics* **2011**, *667*, 85-95.

[8] Devineau, S., Anyfantakis, M., Marichal, L., Kiger, L., Morel, M., Rudiuk, S. and Baigl, D., Protein adsorption and reorganization on nanoparticles probed by the coffee-ring effect: application to single point mutation detection. *Journal of the American Chemical Society* **2016**, *138*(36), 11623-11632.

[9] Lanotte, L., Laux, D., Charlot, B. and Abkarian, M., Role of red cells and plasma composition on blood sessile droplet evaporation. *Physical Review E* **2017**, *96*(5), 053114.

[10] Wen, J. T.; Ho, C.-M.; Lillehoj, P. B., Coffee ring aptasensor for rapid protein detection. *Langmuir* **2013**, *29*, 8440− 8446.

[11] Yakhno, T. A.; Sedova, O. A.; Sanin, A. G.; Pelyushenko, A. S., On the existence of regular structures in liquid human blood serum (plasma) and phase transitions in the course of its drying. *Technical Physics* **2003**, *48*(4), 399–403.

[12] Sobac, B.; Brutin, D., Structural and evaporative evolutions in desiccating sessile drops of blood. *Physical Review E.* **2011**, *84*(1), 011603.

[13] Deegan, R. D.; Bakajin, O.; Dupont, T. F.; Huber, G.; Nagel, S. R.; Witten, T. A., Capillary flow as the cause of ring stains from dried liquid drops. *Nature* **1997**, *389*(6653), 827.

[14] Anyfantakis, M.; Baigl, D., Manipulating the coffee-ring effect: interactions at work. *ChemPhysChem* **2015**, *16*(13), 2726-2734.

[15] Chen, R.; Zhang, L.; Zang, D.; Shen, W., Blood drop patterns: Formation and applications. *Advances in colloid and interface science* **2016**, *231*, 1-14.

[16] Poulichet, V.; Morel, M., Rudiuk, S; Baigl, D., Liquid-liquid coffee-ring effect. *Journal of Colloid and Interface Science* **2020**, *573*, 370-375.

[17] Zang, D.; Tarafdar, S.; Tarasevich, Y. Y.; Choudhury, M. D.; Dutta, T., Evaporation of a Droplet: From physics to applications. *Physics Reports* **2019**, *804*, 1-56.

[18] Thampi, S. P. ; Basavaraj, M. G., Beyond Coffee Rings: Drying Drops of Colloidal Dispersions on Inclined Substrates. *ACS Omega* **2020**, *5*(20), 11262–11270.

[19] Erbil, H. Y., Evaporation of pure liquid sessile and spherical suspended drops: A review. *Advances in colloid and interface science* **2012**, *170*(1-2), 67-86.

[20] Yunker, P. J.; Still, T.; Lohr, M. A.; Yodh, A. G., Suppression of the coffee-ring effect by shape-dependent capillary interactions. *Nature* **2011**, *476*(7360), 308.

[21] Tsapis, N.; Dufresne, E. R.; Sinha, S. S.; Riera, C. S.; Hutchinson, J. W.; Mahadevan, L.; Weitz, D. A., Onset of buckling in drying droplets of colloidal suspensions. *Physical Review Letters* **2005**, *94*(1), 018302.

[21] Tarasevich, Y. Y.; Vodolazskaya, I. V.; Bondarenko, O. P., Modeling of spatial–temporal distribution of the components in the drying sessile droplet of biological fluid. *Colloids and Surfaces A: Physicochemical and Engineering Aspects* **2013**, *432*, 99-103.

[22] Yakhno, T. A.; Yakhno, V. G., Structural evolution of drying drops of biological fluids. *Technical physics* **2009**, *54*(8), 1219-1227.

[23] Yakhno, T., Salt-induced protein phase transitions in drying drops. *Journal of colloid and interface science* **2008**, *318*(2), 225-230.

[24] Gorr, H. M.; Zueger, J. M.; McAdams, D. R.; Barnard, J. A., Salt-induced pattern formation in evaporating droplets of lysozyme solutions. *Colloids and Surfaces B: Biointerfaces* **2013**, *103*, 59-66.

[25] Yakhno, T. A., Sodium chloride crystallization from drying drops of albumin–salt solutions with different albumin concentrations. *Technical Physics* **2015**, *60*(11), 1601-1608.

[26] Tarasevich, Y. Y.; Pravoslavnova, D. M., Drying of a multicomponent solution drop on a solid substrate: Qualitative analysis. *Technical Physics* **2007**, *52*(2), 159-163.

[27] Tarasevich, Y. Y.; Pravoslavnova, D. M., Segregation in desiccated sessile drops of biological fluids. *The European Physical Journal E.* **2007**, *22*(4), 311-314.

[28] Annarelli, C. C.; Reyes, L.; Fornazero, J.; Bert, J.; Cohen, R.; Coleman, A. W., Ion and molecular recognition effects on the crystallization of bovine serum albumin–salt mixtures. *Crystal engineering* **2000**, *3*(3), 173-194.

[29] Sett, A.; Ayushman, M.; Dasgupta, S. ; DasGupta, S., Analysis of the Distinct Pattern Formation of Globular Proteins in the Presence of Micro-and Nanoparticles. *The Journal of Physical Chemistry B* **2018**, *122*(38), 8972-8984.

[30] Kastelic, M.; Kalyuzhnyi, Y. V.; Hribar-Lee, B.; Dill, K. A.; Vlachy, V., Protein aggregation in salt solutions. *Proceedings of the National Academy of Sciences* **2015**, *112*(21), 6766-6770.

[31] Möller, J.; Schroer, M. A.; Erlkamp, M.; Grobelny, S.; Paulus, M.; Tiemeyer, S.; Wirkert, F. J.; Tolan, M.; Winter, R., The effect of ionic strength, temperature, and pressure on the interaction potential of dense protein solutions: from nonlinear pressure response to protein crystallization. *Biophysical journal* **2012**, *102*(11), 2641-2648.

[32] Zhang, F.; Skoda, M. W.; Jacobs, R. M.; Martin, R. A.; Martin, C. M.; Schreiber, F., Protein interactions studied by SAXS: effect of ionic strength and protein concentration for BSA in aqueous solutions. *The Journal of Physical Chemistry B* **2007**, *111*(1), 251-259.

[33] Zhang, B.; Yu, W.; Zhou, L. Q.; He, Z. S.; Shen, C.; He, Q.; Li, J., Liu, L.; Wang, C.; Chen, X.; Fan, Y.; Hu, S., Zhang, L.; Han, W.; Jin, J., Prognostic significance of preoperative albumin-globulin ratio in patients with upper tract urothelial carcinoma. *PloS one* **2015**, *10* (12), e0144961, 1-12.

[34] Liu, J., Dai, Y.; Zhou, F.; Long, Z.; Li, Y.; Liu, B.; Xie, D.; Tang, J.; Tan, J.; Yao, K.; Zhang, Y.; Tang, Y.; He, L., The prognostic role of preoperative serum albumin/globulin ratio in patients with bladder urothelial carcinoma undergoing radical cystectomy. In *Urologic Oncology: Seminars and Original Investigations* **2016**, *34* (11), 484e1-484e8.

[35] Liu, T. L.; Kim, C. C., Contact Angle Measurement of Small Capillary Length Liquid in Super-repelled State. *Scientific reports* **2017**, *7*(1), 740-740.

[36] Yakhno, T. A.; Yakhno, V. G.; Sanin, A. G.; Sanina, O. A.; Pelyushenko, A. S. Protein and salt: spatio-temporal dynamics of events in a drying drop. *Technical Physics* **2004**, *49* (8), 1055-1063.

[37] Chemical Encyclopedia http://www.chemport.ru/data/ chemipedia/article_2342.html

[38] Chen, G.; Mohamed, G.J., Complex protein patterns formation via salt-induced self-assembly and droplet evaporation. *The European Physical Journal E* **2010**, *33* (1), 19-26.

[39] Szabó, B.; Vicsek, T. Protein-induced morphological transitions in KCl crystal growth. *Physical Review E* **2003**, *67*(1), 011908.

[40] Harned, H. S.; Blake, C. A. The diffusion coefficient of potassium chloride in water at 4C. *Journal of the American Chemical Society* **1950**, *72*(5), 2265-2266.

[41] Jones, J. R.; Rowlands, D. L. G.; Monk, C. B. Diffusion coefficient of water in water and in some alkaline earth chloride solutions at 25 C. *Transactions of the Faraday Society* **1965**, *61*, 1384-1388.

For Table of Contents Only